



UNIVERSITY OF LEEDS

This is a repository copy of *Temperature-stable dielectric properties from -20°C to 430°C in the system BaTiO₃-Bi(Mg_{0.5}Zr_{0.5})O₃*.

White Rose Research Online URL for this paper:
<http://eprints.whiterose.ac.uk/83517/>

Version: Accepted Version

Article:

Zeb, A and Milne, SJ (2014) Temperature-stable dielectric properties from -20°C to 430°C in the system BaTiO₃-Bi(Mg_{0.5}Zr_{0.5})O₃. *Journal of the European Ceramic Society*, 34 (13). 3159 - 3166. ISSN 0955-2219

<https://doi.org/10.1016/j.jeurceramsoc.2014.04.047>

Reuse

Unless indicated otherwise, fulltext items are protected by copyright with all rights reserved. The copyright exception in section 29 of the Copyright, Designs and Patents Act 1988 allows the making of a single copy solely for the purpose of non-commercial research or private study within the limits of fair dealing. The publisher or other rights-holder may allow further reproduction and re-use of this version - refer to the White Rose Research Online record for this item. Where records identify the publisher as the copyright holder, users can verify any specific terms of use on the publisher's website.

Takedown

If you consider content in White Rose Research Online to be in breach of UK law, please notify us by emailing eprints@whiterose.ac.uk including the URL of the record and the reason for the withdrawal request.



eprints@whiterose.ac.uk
<https://eprints.whiterose.ac.uk/>

Temperature-Stable Dielectric Properties from -20°C to 430°C in the System $\text{BaTiO}_3\text{-Bi}(\text{Mg}_{0.5}\text{Zr}_{0.5})\text{O}_3$

Aurang Zeb and Steven J. Milne*

Institute for Materials Research, University of Leeds, Leeds LS2 9JT, United Kingdom

*Tel 0113 343 2539

Fax 0113 343 2384

a.zeb@leeds.ac.uk; s.j.milne@leeds.ac.uk

Abstract

Ceramics in the solid solution series $(1-x)\text{BaTiO}_3\text{-Bi}(\text{Mg}_{0.5}\text{Zr}_{0.5})\text{O}_3$ are single-phase tetragonal for compositions $x \leq 0.05$, and cubic for $x \geq 0.1$. Plots of relative permittivity (ϵ_r), versus temperature show double peaks for $x = 0.03$ and $x = 0.05$, changing to a single, frequency-dependent peak for compositions, $x \geq 0.1$. A progressive decline in $\epsilon_{r\text{max}}$ with increasing x leads to near temperature-stable dielectric properties over a wide temperature range. For $x = 0.3$, $\epsilon_r = 570 \pm 15\%$, from -20°C to 430°C , and $\tan \delta \leq 0.02$ from 30°C to 420°C . For $x = 0.4$, $\epsilon_r = 600 \pm 15\%$ from 25°C - 420°C , and $\tan \delta \leq 0.02$ from 55°C to 280°C (at 1 kHz). Values of dc resistivity were $\sim 10^9 \Omega \text{ m}$ at 250°C and $\sim 10^6 \Omega \text{ m}$ at 400°C . A piezoelectric strain of $\sim 0.25\%$ (at 40 kV/cm) was recorded for composition $x = 0.03$.

Introduction

The distinctive properties of classical relaxor dielectrics are broad, frequency-dependent peaks in plots of relative permittivity (ϵ_r) versus temperature, and strong frequency dispersion in dielectric loss tangent ($\tan\delta$) [1-5]. Relaxor characteristics were first discovered by Smolensky and co-workers in lead magnesium niobate (PMN), and there has been strong

interest in these materials in the intervening decades due to their distinctive dielectric and electromechanical properties [2-4, 6].

Several theories have been proposed to account for this behaviour, based on concepts of compositional disorder and the formation of polar nanoregions/domains [3-8]. Most relaxors involve mixed valence multiple cation site occupancy on the B-sites of the perovskite ABO_3 [1, 9-12]. A number of complex perovskites have emerged in recent years, involving mixed valence occupancy of both A and B-sites. These exhibit relaxor-like frequency dependent decreases in ϵ_r at $T < T_m$ but for certain solid solution compositions show little change in ϵ_r values across a wide temperature range, $T > T_m$. The origin of this effect may lie in the suppression of thermally induced changes to the total volume of polar regions as a consequence of the highly defective crystal lattice. These temperature stable relaxor dielectrics are of interest for new types of high volumetric efficiency capacitors operating at > 200 °C for use in electronic systems for aviation, automotive and deep-well drilling applications [12]. Temperature stability, defined here as a variation in relative permittivity of within $\pm 15\%$ (consistent with the EIA classification system 'R'), occurs at higher temperatures than for traditional $BaTiO_3$ based dielectrics such as X7R which is specified at -55 °C to 125 °C.

Promising high temperature dielectric properties have been demonstrated within relaxor complex solid solutions in which $BiScO_3$ is an end-member: examples include $BaTiO_3$ - $BiScO_3$ [13], $K_{0.5}Bi_{0.5}TiO_3$ - $BiScO_3$ [8], $BaTiO_3$ - $BiZn_{0.5}Ti_{0.5}O_3$ - $BiScO_3$ [14] and $Na_{0.5}K_{0.5}NbO_3$ - $LiTaO_3$ - $BiScO_3$ [15, 16]. There are also high temperature dielectrics that are Sc-free, also with Bi^{3+} as one of the mixed A-site substituents, these include $Bi_{0.5}Na_{0.5}TiO_3$ - $BaTiO_3$ - $K_{0.5}Na_{0.5}NbO_3$ [17], $Bi_{0.5}Na_{0.5}TiO_3$ - $BaTiO_3$ - $CaZrO_3$ [18], $Ba_{0.8}Ca_{0.2}TiO_3$ - $Bi(Mg_{0.5}Ti_{0.5})O_3$ [6]; $Ba_{0.8}Ca_{0.2}TiO_3$ - $Bi(Mg_{0.5}Ti_{0.5})O_3$ - $NaNbO_3$ [12] and $BaTiO_3$ - $Bi(Zn_{0.5}Zr_{0.5})O_3$ [19].

The ternary system $\text{BaTiO}_3\text{-Bi}(\text{Zn}_{0.5}\text{Ti}_{0.5})\text{O}_3\text{-BiScO}_3$ at the composition 50BT-25BZT-25BS (with 2 mol% Ba-deficiency) is reported with $\epsilon_r = 1120 \pm 10$ % over the temperature range $\leq 100\text{-}450$ °C [14]. However, the very high price of scandium oxide limits its commercial applications: 50BT-25BZT-25BS contains ~10 wt% Sc_2O_3 . An alternative and low-cost system, $(1-x)\text{Ba}_{0.8}\text{Ca}_{0.2}\text{TiO}_3\text{-xBi}(\text{Mg}_{0.5}\text{Ti}_{0.5})\text{O}_3$ has $\epsilon_r = 830 \pm 10$ % and low, $\tan \delta \leq 0.02$, from $\sim 50^\circ\text{C}$ to 550 °C for composition $x = 0.5$; $\epsilon_r = 950 \pm 10$ % over the wide temperature range from $+80$ °C to 600 °C for composition $x = 0.45$ [6,12,28]. The end member $\text{Bi}(\text{Mg}_{0.5}\text{Ti}_{0.5})\text{O}_3$ is of rhombohedral structure at room temperature, with $T_c \sim 430$ °C but can only be prepared at high pressure (6 GPa) at a temperature ~ 1000 °C [20, 21]. However, it forms useful solid solutions under normal processing conditions with a number of other perovskites [6, 20-22]. The system $\text{Bi}(\text{Mg}_{0.5}\text{Ti}_{0.5})\text{O}_3\text{-BaTiO}_3$ (BMT-BT) [20] exhibits a near temperature stable ϵ_r response ($\epsilon_r \sim 2400 \pm 15\%$) across the temperature range $167\text{-}400$ °C for composition 50 BMT-50 BT. However, low dielectric loss ($\tan \delta \leq 0.02$) only occurs between $238\text{-}400$ °C [20].

In the present study, we report the phase stability, dielectric response and dc resistivity of another perovskite ceramic with mixed A and B-site occupancy, formed in the compositional system $(1-x)\text{BaTiO}_3\text{-xBi}(\text{Mg}_{0.5}\text{Zr}_{0.5})\text{O}_3$ (abbreviated; BT-BMZ). Promising temperature insensitive dielectric properties at elevated temperatures are demonstrated for $x = 0.3$ and 0.4 compositions which have a more extended temperature range of operation compared to most alternative materials, with a ± 15 % variation in ϵ_r from temperatures of $\text{minus } 20$ °C to 430 °C for $x = 0.3$, and for $x = 0.4$, from 25°C to 420°C .

Experimental procedure

Ceramic samples in the $(1-x)\text{BaTiO}_3\text{-xBi}(\text{Mg}_{0.5}\text{Zr}_{0.5})\text{O}_3$ system were prepared by a conventional solid state processing route for compositions $x \leq 0.6$ using reagent grade

powders: BaCO₃ (Alpha Aesar, 99%, Ward Hill MA), Bi₂O₃ (Alpha Aesar, 99%, Ward Hill MA), TiO₂ (Sigma Aldrich, 99.9% purity, St. Louis, MO), MgO (Alpha Aesar, 99.9%), ZrO₂ (Dynamic ceramic, Crewe Hall, UK). The powders were dried overnight at 250 °C and cooled to room temperature followed by weighing according to stoichiometric proportions. The weighed powders were ball milled using zirconia-based grinding media in isopropanol for 24 h. The dried slurries, after sieving through a 300 µm mesh nylon sieve, were calcined at 900 °C for 4 h in closed alumina crucibles with heating and cooling ramp rates of 300 °C/h. The calcined powders were re-milled for 24 h, and 1% wt binder was added (Ciba Glascol HA4: Ciba speciality Chemicals, Bradford, UK). The powders were again sieved through a 300 µm mesh nylon sieve, compacted into pellets ~ 10 mm diameter and ~1.5 mm in thickness in a steel die by applying a uniaxial pressure of 65 MPa, followed by cold isostatic pressing at 200 MPa.

Sintering was carried out at temperatures ranging from 1000 °C - 1350 °C for 6 h in air; the optimum temperature depended on composition (lower sintering temperatures were required for the higher BMZ content samples), given in Table 1. Pellets were placed in closed alumina crucibles and surrounded by powder of the same composition in order to minimise the loss of volatile oxides from the pellets. The phase content of sintered pellets was analysed using x-ray powder diffraction (XRD, Bruker D8, Cu, K α ~1.5406 Å, scan speed, 1°/min Karlsruhe, Germany;) after crushing and grinding the pellets to a powder. Lattice parameters were calculated using the least squares refinement method. Microstructural information on polished and chemically etched samples was obtained using transmission electron microscopy (TEM; Philips, CM200) and scanning electron microscopy (SEM; Leo 1530). Grain size was estimated using the linear intercept method. Density was measured geometrically; theoretical density was estimated from lattice parameters and unit cell contents.

For electrical property measurements, the sintered pellets were ground and polished to ~1 mm thickness; electrodes were applied to opposite parallel faces using silver paste (Agar Scientific) fired at 550 °C for 10 min. The dielectric relative permittivity and loss tangent were measured as a function of temperature over the range ~25 °C to 600 °C by using an impedance analyzer (HP Agilent, 4192A Hewlett Packard, Santa Clara, CA). The values of dc resistance were recorded as a function of temperature in the range ~200 °C-550 °C at a fixed dc voltage of 80 V, using a Keithley 617 programmable electrometer (Cleveland, OH). The polarisation-electric field, P-E, and strain-field, S-E, response were measured at room temperature using a LC precision analyzer (Radiant Technologies Inc., Albuquerque, New Mexico).

Results and Discussion

Figure 1, shows the X-ray diffraction patterns of $(1-x)\text{BaTiO}_3-x\text{Bi}(\text{Mg}_{0.5}\text{Zr}_{0.5})\text{O}_3$ samples. Peaks due to the secondary phase ($\text{Bi}_{12}\text{MgO}_{19}$) appeared in the $x = 0.5$ pattern and increased in intensity at $x = 0.6$ [23]. Therefore, no samples with $x > 0.6$ were prepared. Compositions $x \leq 0.05$ were tetragonal perovskite; the 200 reflection for $x = 0.05$ showed a high angle shoulder but no clear evidence of peak splitting, whilst the XRD patterns for $x \geq 0.1$ were cubic. The lattice parameters are plotted as a function of x in Figure 2, illustrating a contraction in tetragonal distortion between $x = 0$ and 0.03.

The microstructure of selected sintered pellets is shown in Figure 3, indicating a decrease in grain size due to the incorporation of BMZ. Information on sintering temperatures (optimised for each composition) pellet density and grain size are summarised in Table 1.

Figure 4 shows the temperature dependence of relative permittivity and dielectric loss tangent ($\tan\delta$) measured at various frequencies (1 kHz, 10 kHz, 100 kHz and 1 MHz) from room temperature to 600 °C. The incorporation of BMZ transformed the dielectric response from a

ferroelectric with a sharp Curie peak at ~ 130 °C for BaTiO₃ ($x = 0$), Fig 4a, to double, broad dielectric peaks for $x = 0.03$, with $\epsilon_{r \text{ peak1}} = 2900$ at $T_{m1} = 115$ °C and $\epsilon_{r \text{ peak2}} = 2700$ at $T_{m2} = 150$ °C, with a weak frequency dependence in T_{m1} , in the $x = 0.03$ sample, Fig 4b. The $x = 0.05$ sample also displayed twin peaks with an increased dispersion in T_{m1} , and a decrease in T_{m1} to 30 °C, Fig 4c. The temperature of the second peak, T_{m2} , in $x = 0.05$ was similar to that of $x = 0.03$ (~ 150 °C), but the relative size of the peak was diminished. Analysis by TEM-EDX of $x = 0.05$ indicated a core-shell structure in many grains, with a shell rich in Bi, Mg and Zr relative to the grain interior, Figure 5. Hence the double peaks in ϵ_r -T plots may be attributed to two different compositions, the general trends in peak temperatures infer the shell is similar to the target composition and gives rise to the ϵ_r -peak at T_{m1} whilst the higher temperature peak, $T_{m2} \sim 150$ °C, is attributed to the core (rich in Ba and Ti). Double ϵ_r peaks and core shell elemental segregation have been reported in other perovskite solid solutions [13, 15, 24].

Increasing the BMZ content to $x = 0.1$ produced a single, broad relaxor dielectric peak, with $T_m \leq 20$ °C (1 kHz) and a reduction in $\epsilon_{r \text{ max}}$ to ~ 1400 , Figure 4d. The relative permittivity at 400 °C in $x = 0.1$ remained similar to $x = 0.03$ and 0.05 samples. Further increases in x continued to decrease $\epsilon_{r \text{ max}}$ creating a drop in the rate of change in ϵ_r with temperature at $T > T_m$. At $x = 0.3$ the temperature variation in ϵ_r lay within $\pm 10\%$ of a mid- value of 570 from -15 °C to 400 °C and $\tan \delta$ values were ≤ 0.02 across the temperature range 30 °C to 420 °C. For $x = 0.4$, $\epsilon_r = 600 \pm 10\%$ from 25 °C-400 °C, however, at temperatures > 280 °C dielectric losses increased sharply. The reason for the higher dielectric losses is thought to relate to dc conduction which increases more sharply at high temperatures in samples with higher Bi contents due to the bismuth oxide volatilisation [24- 27].

A summary of the dielectric data for all samples is presented in Table 2. These are useful properties but as with most of the new breed of high temperature dielectric ceramics, the

stable performance does not extend to the sub-zero temperatures. Exceptions include Ba,CaTiO_{3-x}Bi(Mg_{0.5}Ti_{0.5})O₃-NaNbO₃ [18, 28].

The frequency dispersion of relaxor samples was considered in terms of the Vögel-Fulcher relationship [8] expressed as,

$$f = f_o \exp\left(\frac{-E_a}{k_B(T_m - T_f)}\right) \quad (1)$$

where f is the measured frequency, f_o is the attempt frequency, E_a represents the activation energy, k_B is the Boltzmann constant, and T_m is the temperature of maximum relative permittivity. The parameter T_f is the Vögel-Fulcher freezing temperature that is considered the temperature below which there is orientational freezing of interactions between polar nanoregions or domains in a relaxor [8, 29]. The obtained values of freezing temperature T_f , activation energy E_a and attempt frequency f_o are listed in the **Table 3** (Vögel-Fulcher fit $R^2 \sim 0.998$), and compared with other related perovskites ceramic materials [8, 13, 14, 30-32]. The samples with dielectric plateau ($x = 0.3- 0.4$) demonstrated freezing temperatures of 70-80 K slightly lower than values reported for the weakly coupled relaxor BaTiO₃-BiScO₃ and similar to Bi-modified SrTiO₃ [29].

Figure 6 displays dc resistivity values as a function of temperature, measured at a fixed voltage of ~80 V for $x = 0.05$ and $x = 0.4$ from 200 °C - 550 °C. There was a decrease in resistivity with increasing x , most notably toward the lower range of temperatures. For $x = 0.4$ values of resistivity were of the order of $10^6 \Omega \text{ m}$ at 400 °C and $10^9 \Omega \text{ m}$ at 250 °C. A change in slope of resistivity plots was observed at ~320 °C, corresponding to a change in activation energy of the electrical conduction process [33-37]. For $x=0.05$, activation energy, $E_a = 0.54 \text{ eV}$ in the low temperature region ($< 325 \text{ °C}$) and 0.68 eV at higher temperatures. Values of low-temperature E_a , were 0.49 eV for $x = 0.4$ with corresponding high temperature

$E_a = 0.64$. These values fall in the range normally associated with the migration of oxygen lattice vacancies [33-35].

Polarisation-electric field hysteresis loops measured at room temperature are shown in Figures 7a and b. Solid solution samples $x = 0.03$ and 0.05 displayed ferroelectric P-E loops. There was a contraction of the P-E loops as x increased from 0 to 0.03 to 0.05 and a decreased polarisation. For $x \geq 0.1$ there was no evidence of domain switching in P-E loops; the response being that of a capacitor with very low leakage current for $x = 0.3$ and 0.4 , Figure 7b. The electric field induced strain behaviour is shown in Figure 8. The ferroelectric composition $x = 0.03$, close to the tetragonal-pseudocubic phase boundary, with ϵ_r peak at 115°C , gave a strain at room-temperature of $\sim 0.25\%$ (at 40kV/cm)- this is a relatively high value for a Pb-free piezoelectric [38-41]. The $x = 0.05$ sample, with a ϵ_r peak at 30°C demonstrated an electrostrictive strain of 0.32% .

Conclusions

Ceramic compositions in the $(1-x)\text{BaTiO}_3\text{-}x\text{Bi}(\text{Mg}_{0.5}\text{Zr}_{0.5})\text{O}_3$ system, for compositions $x < 0.6$ have been fabricated by conventional ceramic processing techniques. At low levels of $\text{Bi}(\text{Mg}_{0.5}\text{Zr}_{0.5})\text{O}_3$ substitution, $x = 0.03$ and 0.05 , a double peak was observed in plots of relative permittivity versus temperature. A change to normal relaxor dielectric plots, with a single, broad frequency dependent relative permittivity peak occurred at $x = 0.1$. At $x = 0.3$ and 0.4 the peak relative permittivity value decreased such that a low variation in relative permittivity was observed. The values of ϵ_r were in the range $600 \pm 10\%$ from 25°C to 400°C for $x = 0.4$ (at 1 kHz). The dc resistivity values were of the order of $10^9\ \Omega\ \text{m}$ at 250°C and $10^6\ \Omega\ \text{m}$ at 400°C . The ferroelectric $x = 0.03$ solid solution, close to the tetragonal pseudocubic phase boundary, with a ϵ_r peak temperature of 115°C , gave a piezoelectric strain of $\sim 0.25\%$ (at 40kV/cm)

Acknowledgments

Aurang Zeb wishes to thank the government of Pakistan (HEC and Islamia College Peshawar, Chartered University) for providing funds (Scholarship). Thanks are expressed to Tim Button and Yang Bai, University of Birmingham, UK for low temperature dielectric measurements.

References:

1. Bokov AA and Ye Z.-G. Recent Progress in Relaxor Ferroelectrics with Perovskite Structure. *J. Mater. Sci.*, 2006; **41**[1]: 31-52.
2. Wang H-C and Schulze WA. The Role of Excess Magnesium Oxide or lead Oxide in Determining the Microstructure and Properties of Lead Magnesium Niobate. *J. Am. Ceram. Soc.*, 1990; **73** [4]: 825-32.
3. Shvartsman VV and Lupascu DC. Lead-Free Relaxor Ferroelectrics. *J. Am. Ceram. Soc.*, 2012; **95** [1]: 1–26.
4. Laulhé C, Hippert F, Kreisel J, Maglione M, Simon A, Hazemann JL, and Nassif V. EXAFS study of lead-free relaxor ferroelectric $\text{BaTi}_{1-x}\text{Zr}_x\text{O}_3$ at the Zr K edge. *Phys. Rev. B.*, 2006; **74**:014106(1-12).
5. Badapanda T, Rout SK, Cavalcante LS, Sczancoski JC, Panigrahi S, Longo E and Li MS. Optical and dielectric relaxor behaviour of $\text{Ba}(\text{Zr}_{0.25}\text{Ti}_{0.75})\text{O}_3$ ceramic explained by means of distorted clusters. *J. Phys. D: Appl. Phys.*, 2009; **42**:175414(1-9).
6. Zeb A and Milne SJ. Stability of High-Temperature Dielectric Properties for $(1-x)\text{Ba}_{0.8}\text{Ca}_{0.2}\text{TiO}_3-x\text{Bi}(\text{Mg}_{0.5}\text{Ti}_{0.5})\text{O}_3$ Ceramics. *J. Am. Ceram. Soc.*, 2013; **96**[9]: 2887-2892.
7. Bokov AA and Ye Z.-G. Phenomenological description of dielectric permittivity peak in relaxor ferroelectrics. *Solid State Commun.*, 2000; **116**:105–108.

8. Kruea-In C, Rujijanagul G, Zhu F and Milne SJ. Relaxor Behaviour of $K_{0.5}Bi_{0.5}TiO_3$ - $BiScO_3$ Ceramics. *Appl. Phys. Lett.*, 2012; **100**: 202904(1-4).
9. Smolensky G. Ferroelectrics with diffuse phase transition. *Ferroelectrics*; 1984; **53**[1]: 129-135.
10. Ravez J and Simon A. Some Solid State Chemistry Aspects of Lead-Free Relaxor Ferroelectrics. *J. Solid State Chem.*, 2001; **162**: 260-265.
11. Bokov AA. Recent advances in diffuse ferroelectric phase transitions. *Ferroelectrics*; 1992: **131**[1]: 49-55.
12. Zeb A and Milne SJ. Dielectric properties of $Ba_{0.8}Ca_{0.2}TiO_3$ - $Bi(Mg_{0.5},Ti_{0.5})O_3$ - $NaNbO_3$ ceramics. *J. Am. Ceram. Soc.*, 2013; **96** [12]: 3701-3703.
13. Ogihara H, Randall CA, and Trolier-McKinstry S. Weakly Coupled Relaxor Behaviour of $BaTiO_3$ - $BiScO_3$ Ceramics. *J. Am. Ceram. Soc.*, 2009; **92** [1] 110–118.
14. Raengthon N, Sebastian T, Cumming D, Reaney IM and Cann DP. $BaTiO_3$ - $Bi(Zn_{0.5}Ti_{0.5})O_3$ - $BiScO_3$ Ceramics for high-temperature capacitor applications. *J. Am. Ceram. Soc.*, 2012; **95** [11]: 3554-3561.
15. Zhu F, Skidmore TA, Bell AJ, Comyn TP, James CW, Ward M, and Milne SJ. Diffuse Dielectric Behaviour in $Na_{0.5}K_{0.5}NbO_3$ - $LiTaO_3$ - $BiScO_3$ Lead-Free Ceramics. *J. Mats. Chem. Phys.*, 2011; **129**: 411–417.
16. Skidmore TA, Comyn TP and Milne SJ. Dielectric and piezoelectric properties in the system: $(1-x)[(Na_{0.5}K_{0.5}NbO_3)_{0.93}-(LiTaO_3)_{0.07}]-x[BiScO_3]$. *J. Am. Ceram. Soc.*, 2010; **93**[3]: 624-626.
17. Dittmer R, Jo W, Damjanovic D and Rödel J. Lead-free high-temperature dielectrics with wide operational range. *J. Appl. Phys.*, 2011; **109**: 034107(1-5).
18. Acosta M, Zang J, Jo W, and Rödel J. High-temperature dielectrics in $CaZrO_3$ -modified $Bi_{1/2}Na_{1/2}TiO_3$ -based lead-free ceramics. *J. Eur. Ceram. Soc.*, 2012; **32**: 4327-4334.

19. Wang Y, Chen X, Zhou H, Fang L, Liu L, Zhang H. Evolution of phase transformation behaviour and dielectric temperature stability of BaTiO₃-Bi(Zn_{0.5}Zr_{0.5})O₃ Ceramic System. *J. Alloy. Compd.*, 2013; **551**: 365–369.
20. Zhang Q, Li Z, Li F, Xu Z. Structural and Dielectric Properties of Bi(Mg_{0.5}Ti_{0.5})O₃ - BaTiO₃ Lead-Free Ceramics. *J. Am. Ceram. Soc.*, 2011; **94**[12]: 4335–4339.
21. Wada S, Yamato K, Pulpan P, Kumada N, Lee B-Y. Preparation of barium titanate-bismuth magnesium titanate ceramics with high Curie temperature and their piezoelectric properties. *Jpn. J. Ceram. Soc.*, 2010; **118**[8]: 683-687.
22. Xiong B, Hao H, Zhang S, Liu H, Cao M. Structure, Dielectric Properties and Temperature Stability of BaTiO₃-Bi(Mg_{0.5}Ti_{0.5})O₃ Perovskite Solid Solutions. *J. Am. Ceram. Soc.*, 2011; **94** [10]: 3412–3417.
23. International Committee for Diffraction Data. Magnesium Bismuth Oxide. 00-042-0302.
24. Skidmore TA, Comyn TP, Bell AJ, Zhu F, and Milne SJ. Phase Diagram and Structure-Property Relationships in the Lead-Free Piezoelectric System: Na_{0.5}K_{0.5}NbO₃-LiTaO₃. *IEEE Transactions on Ultrasonics Ferroelectrics, and Freq. Control*; 2011; **58** [9]: 1819-1825.
25. Bomlai P, Sinsap P, Muensit S. et al. Effect of MnO on the phase development, microstructures, and dielectric properties of 0.95Na_{0.5}K_{0.5}NbO₃-0.05LiTaO₃ ceramics. *J. Am. Ceram. Soc.*, (2008); **91**[2]: 624-627.
26. Bongkarn T, Rujijanagul G, Milne SJ. Effect of excess PbO on phase formation and properties of (Pb_{0.90}Ba_{0.10})ZrO₃ ceramics *Matts. Letts.*, 2005; **59** [10]: 1200-1205.
27. Bongkarn T, Rujijanagul, G, Milne SJ. Antiferroelectric-ferroelectric phase transitions in Pb_{1-x}Ba_xZrO₃ ceramics: Effect of PbO content *Appl. Phys. Letts.*, 2008; **92**[9]: 092905.

28. Zeb A, Bai Y, Button T, Milne SJ. Temperature-stable Relative Permittivity from -70 °C to 500 °C in $(\text{Ba}_{0.8}\text{Ca}_{0.2})\text{TiO}_3\text{-Bi}(\text{Mg}_{0.5}\text{Ti}_{0.5})\text{O}_3\text{-NaNbO}_3$ Ceramics. *J. Am. Ceram. Soc.*, (in press).
29. Stringer CJ, Shrout TR and Randall CA. High Temperature perovskite relaxor ferroelectrics: A comparative study. *J. Appl. Phys.*, 2007; **101**: 054107(1-6).
30. Chen A and Yu Z. Dielectric relaxor and ferroelectric relaxor; Bi-doped Paraelectric SrTiO_3 . *J. Appl. Phys.*, 2002; **91**[3]:1487-1497.
31. Ang C, Jing Z and Yu Z. Ferroelectric relaxor $\text{Ba}(\text{Ti,Ce})\text{O}_3$. *J. Phys. Condens. Matter*; 2002; **14**: 8901-12.
32. Guo HY, Lei C, and Ye Z.-G. Re-entrant type relaxor behaviour in $(1-x)\text{BaTiO}_3\text{-}x\text{BiScO}_3$ solid solution. *Appl. Phys. Lett.*, 2008; **92**: 172901(1-3).
33. Selvamani R, Singh G, Tiwari VS, Gupta PK. Oxygen vacancy related relaxation and conduction behaviour in $(1-x)\text{NBT-xBiCrO}_3$ solid solution. *Phys. Status Solidi., A*; 2012; **209**:118-125.
34. Morrison FD, Sinclair DC, West AR. Electrical and structural characteristics of lanthanum-doped barium titanate ceramics. *J. Appl. Phys.*, 1999; **86**:6355-66.
35. Zeb A and Milne SJ. Low variation in relative permittivity over the temperature range 25-450 °C for ceramics in the system $(1-x) [\text{Ba}_{0.8}\text{Ca}_{0.2}\text{TiO}_3]\text{-}x[\text{Bi}(\text{Zn}_{0.5}\text{Ti}_{0.5})\text{O}_3]$. *J. Eur. Ceram. Soc.*, 2014; **34**:1727-1732.
36. Milne SJ, West AR. Conductivity of Zr-Doped Na_3PO_4 – a new Na^+ Ion Conductor *Mats. Res. Bull.*, 1984; **19** [6]: 705-710 .
37. Milne SJ, West AR. Compound formation and conductivity in the system $\text{Na}_2\text{O-ZrO}_2\text{-P}_2\text{O}_5$ *Solid State Ionics*; 1983; **9-10**: 865-868.

38. Skidmore TA, Comyn, TP, Milne, SJ. Temperature stability of $([\text{Na}_{0.5}\text{K}_{0.5}\text{NbO}_3]_{(0.93)}-[\text{LiTaO}_3]_{(0.07)})$ lead-free piezoelectric ceramics. Appl. Phys. Letts., 2009; **94** [22]: 222902.
39. Royles AJ, Bell AJ, Jephcoat, AP, et al. Electric-field-induced phase switching in the lead free piezoelectric potassium sodium bismuth titanate. Appl. Phys. Letts., 2010; **97**[13]: 132909.
40. Zhu F, Ward MB, Comyn TP, Bell AJ, Milne SJ. Dielectric and piezoelectric properties in the lead- free system $\text{Na}_{0.5}\text{K}_{0.5}\text{NbO}_3\text{-BiScO}_3\text{-LiTaO}_3$. IEEE Trans Ultrason Ferroelectric Freq. Control., 2011; **58**[9]: 1811-1818.
41. Coondoo I, Panwar N, Kholkin A. Lead-free piezoelectrics: Current status and future perspectives. J. Adv. Dielectrics., 2013; **3** [2]: 1330002(1-22).

List of Figures

Figure 1. XRD patterns at room temperature for compositions $x=0-0.5$.

Figure 2. Lattice parameters as a function of BMZ content for $(1-x)\text{BaTiO}_3-x\text{Bi}(\text{Mg}_{0.5}\text{Zr}_{0.5})\text{O}_3$ perovskite solid solution.

Figure 3. SEM micrographs of selected compositions in the $(1-x)\text{BaTiO}_3-x\text{Bi}(\text{Mg}_{0.5}\text{Zr}_{0.5})\text{O}_3$ system (a) $x = 0$; (b) $x = 0.2$; (c) $x = 0.3$; (d) $x = 0.4$

Figure 4. Temperature dependent relative permittivity (ϵ_r) and loss tangent ($\tan\delta$) for compositions (a) $x=0$, (b) $x=0.03$, (c) $x=0.05$, (d) $x=0.1$, (e) $x=0.3$ (inset plot shows relative permittivity at temperature from $-70\text{ }^\circ\text{C}$ to $70\text{ }^\circ\text{C}$) and (f) $x=0.4$.

Figure 5. TEM-dark field image and EDX mapping of elements showing core-shell grain structures, with enhancement of Bi, Mg, Zr in the outer shell for composition $x = 0.05$.

Figure 6. Plots of log dc resistivity as a function of inverse temperature $1000/T(\text{K}^{-1})$ for $x=0.05$ and 0.4 .

Figure 7. Polarisation-electric field, P-E, loops for (a) $x=0-0.05$ and (b) $x=0.2-0.4$.

Figure 8. Electric field–strain behaviour for compositions $x=0.03, 0.05, 0.2$ and 0.4 .

Table 1, Sintering temperatures, density and average grain size of $(1-x)\text{BaTiO}_3-x\text{Bi}(\text{Mg}_{0.5}\text{Zr}_{0.5})\text{O}_3$ ceramics

Table 2. Summary of dielectric properties of $(1-x)\text{BaTiO}_3-x\text{Bi}(\text{Mg}_{0.5}\text{Zr}_{0.5})\text{O}_3$ solid solutions

Table 3. Vögel-Fulcher fitting parameters at 1 kHz, for $x=0.05, 0.1, 0.3$ and 0.4 , in comparison to other perovskite ceramic materials.

Table 1. Sintering temperatures, density and average grain size of $1-x\text{BaTiO}_3-x\text{Bi}(\text{Mg}_{0.5}\text{Zr}_{0.5})\text{O}_3$ ceramics

Sample (x)	Sintering Temperature (°C)	Geometric density (g/cm³)	Relative density (%)	Average grain size (μm)
0.0	1350	5.7	95	10
0.05	1320	5.5	95	3
0.1	1290	5.4	90	4
0.2	1220	6.0	94	7
0.3	1160	6.1	94	6
0.4	1040	6.2	93	5
0.5	1000	6.1	90	5

Table 2. Summary of dielectric properties of BaTiO₃-xBi(Mg_{0.5}Zr_{0.5})O₃ solid solutions

	T_m/ °C	ε_{r max}	T-range/°C tanδ ≤ 0.02	$\frac{\Delta\varepsilon}{\varepsilon_{\text{mid}}} \leq \pm 10\%$	T- range/°C $\frac{\Delta\varepsilon}{\varepsilon_{\text{mid}}} \leq \pm 10\%$	T-range/°C $\frac{\Delta\varepsilon}{\varepsilon_{\text{mid}}} \leq \pm 15\%$
x=0	127	8362	30-215	-	-	
0.03	T_{m1}=115, T_{m2}=150	ε_{r1}= 2900 ε_{r2}= 2700	100-220	-	-	
0.05	T_{m1}=30, T_{m2}=150	ε_{r1}=3300 ε_{r2}=2300	≤25-300	-	-	
0.1	≤25	1440	≤25-350	-	-	
0.2	≤25	660	≤25-380	-	-	
0.3	20	630	30-420	570±10%	-15-400	-20-430
0.4	60	650	55-280	600±10%	25-400	25-420
0.5	70	570	75-250	460±10%	55-400	50-420

Table 3. Vögel-Fulcher fitting parameters at 1 kHz, for x=0.05, 0.1, 0.3 and 0.4, in comparison to other perovskite ceramic materials.

Material	T_{VF}(K)	f_o (Hz)	E_a(eV)	T_m(K)	Reference
0.95BT-0.05BMZ	294	1.0×10^8	0.013	303	This work
0.9BT-0.1BMZ	276	1.6×10^7	0.015	298	
0.7BT-0.3BMZ	70	6.64×10^{10}	0.34	293	
0.6BT-0.4BMZ	80	1.06×10^{12}	0.44	333	
0.80KBT-0.20BS	410	2.2×10^{11}	0.28	540	8
50BT-25BZT-25BS	135	9.6×10^{13}	0.44	-	14
Sr_{1-1.5x}Bi_xTiO₃, x=0.0133	31	1.00×10^{10}	0.036	-	30
Ba(Ti_{0.94}Ce_{0.06})O₃	374	1.45×10^{11}	0.0039	-	31
90BT-10BS	126	5.42×10^{10}	0.15	-	32
90BT-10BS	100	5.5×10^{13}	0.24	-	13

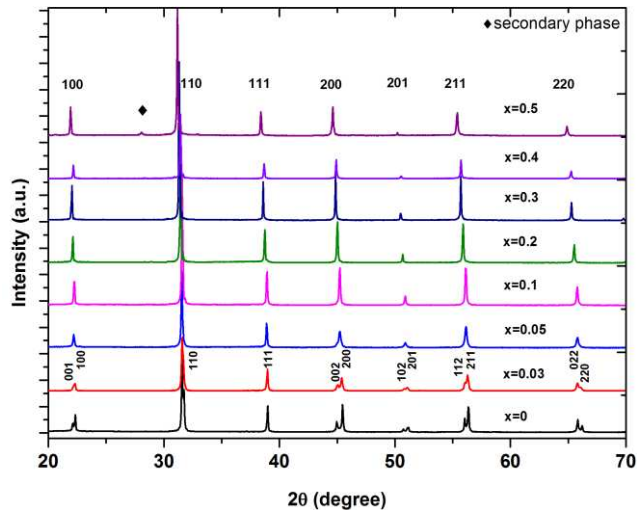


Figure 1. XRD patterns at room temperature for compositions $x=0-0.5$.

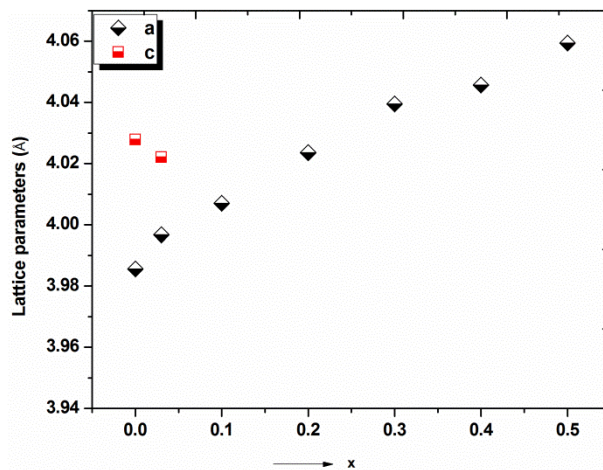


Figure 2. Lattice parameters as a function of BMZ content for $(1-x)\text{BaTiO}_3-x\text{Bi}(\text{Mg}_{0.5}\text{Zr}_{0.5})\text{O}_3$ perovskite solid solution.

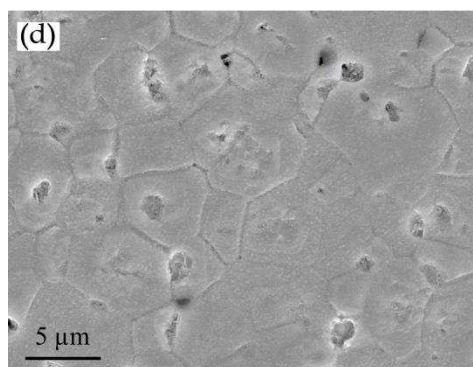
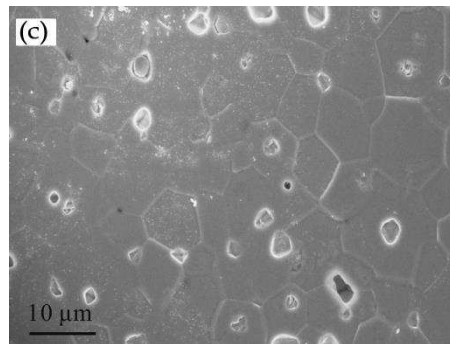
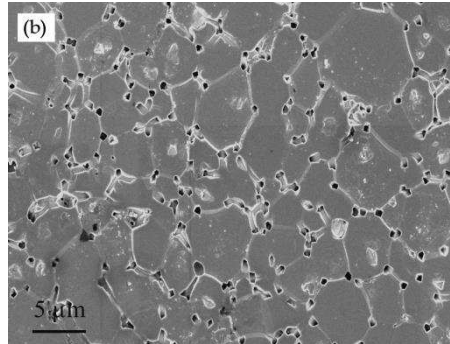
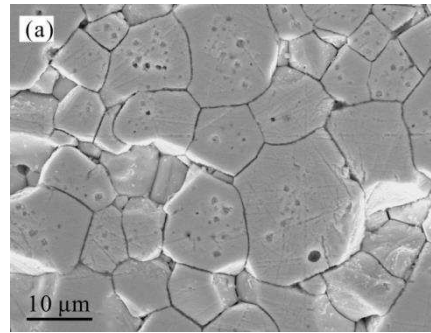
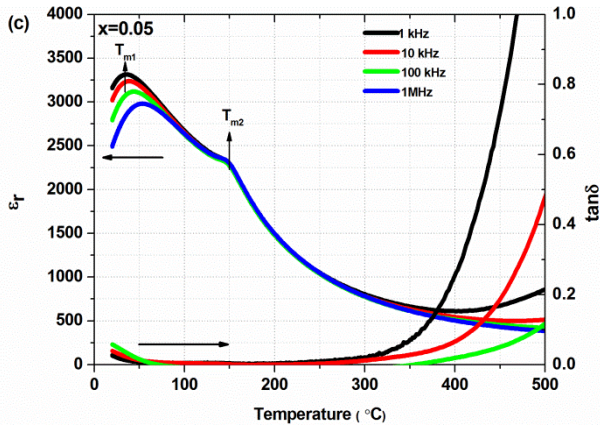
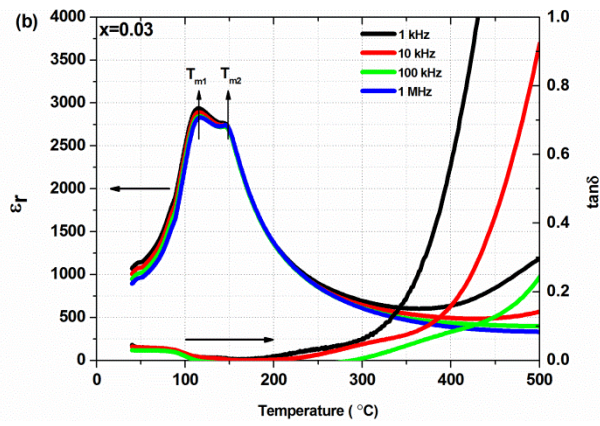
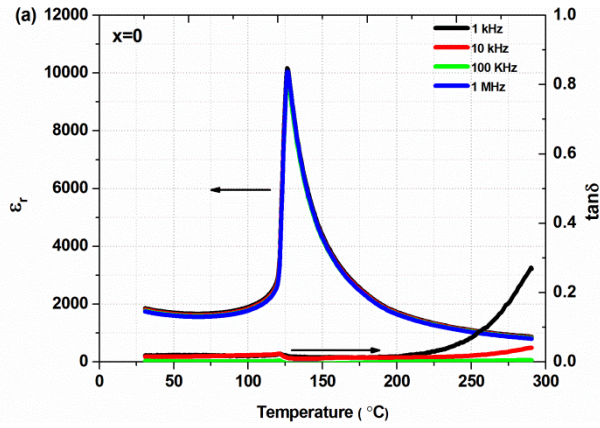


Figure 3. SEM micrographs of selected compositions in the $(1-x)\text{BaTiO}_3-x\text{Bi}(\text{Mg}_{0.5}\text{Zr}_{0.5})\text{O}_3$

system (a) $x = 0$; (b) $x = 0.2$; (c) $x = 0.3$; (d) $x = 0.4$



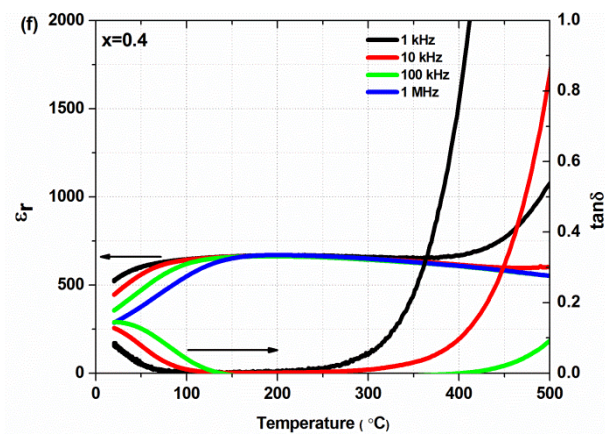
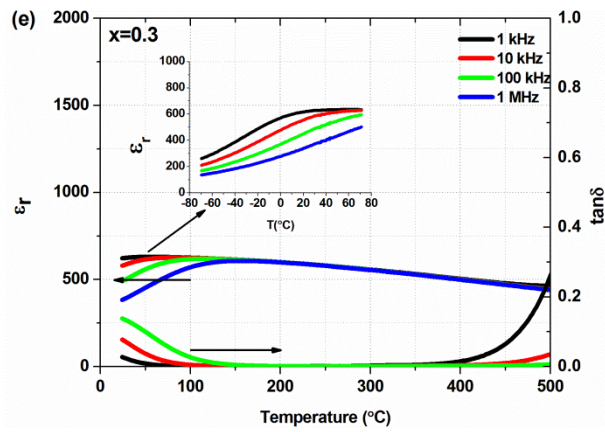
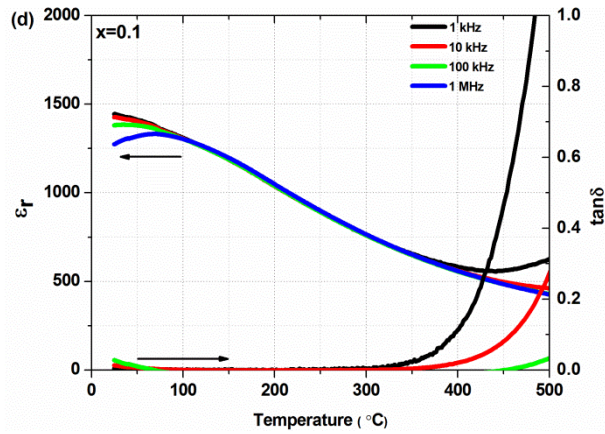


Figure 4. Temperature dependent relative permittivity (ϵ_r) and loss tangent ($\tan\delta$) for compositions (a) $x=0$, (b) $x=0.03$, (c) $x=0.05$, (d) $x=0.1$, (e) $x=0.3$ (inset plot shows relative permittivity at temperature from $-70\text{ }^\circ\text{C}$ to $70\text{ }^\circ\text{C}$) and (f) $x=0.4$.

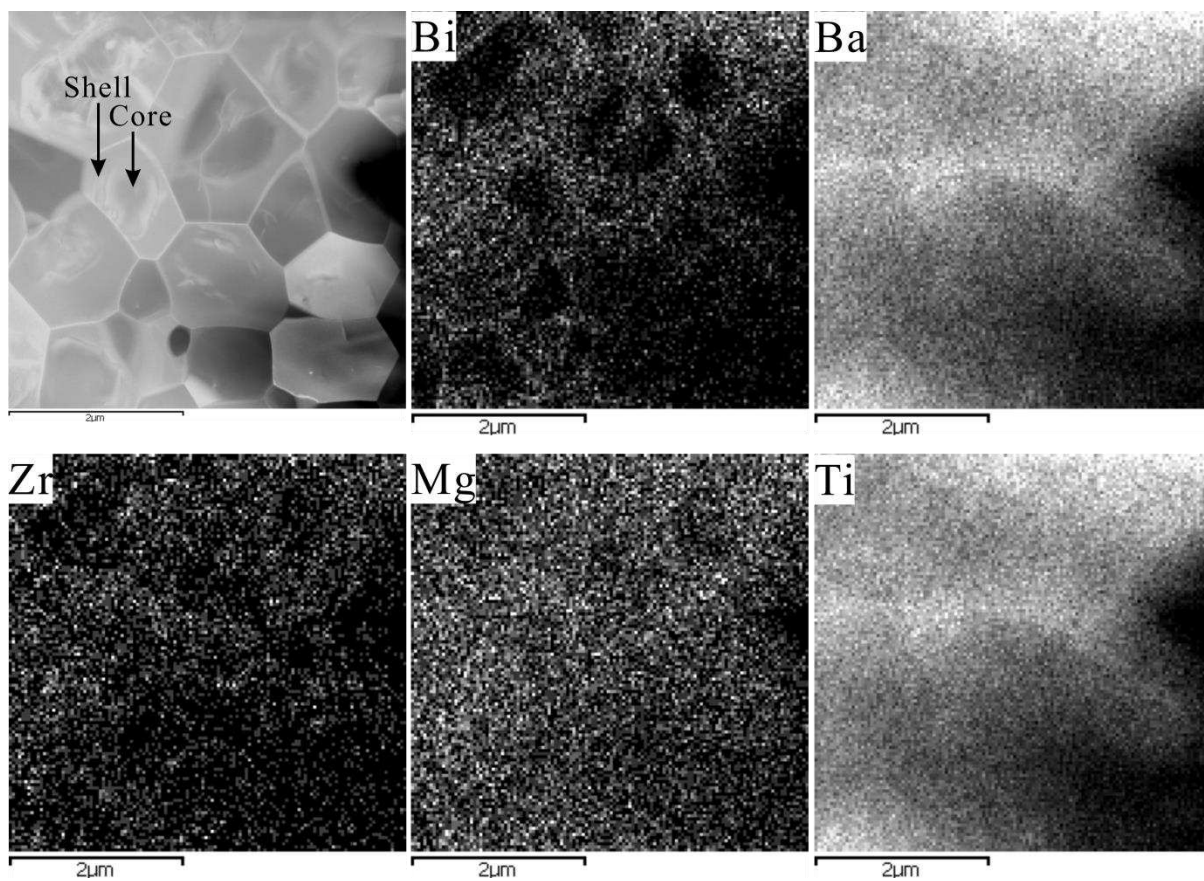


Figure 5. TEM-dark field image and EDX mapping of elements showing core-shell grain structures, with enhancement of Bi, Mg, Zr in the outer shell for composition $x = 0.05$.

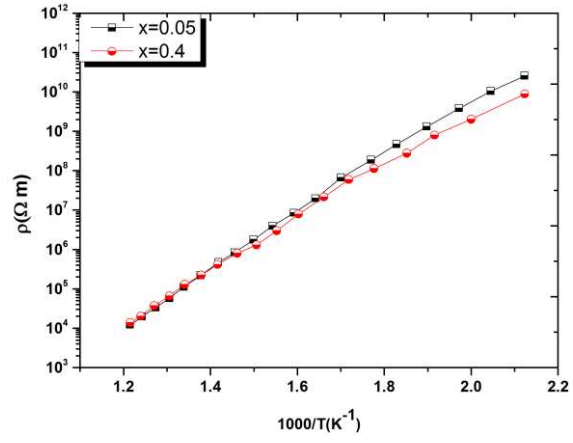


Figure 6. Plots of log dc resistivity as a function of inverse temperature $1000/T(K^{-1})$ for $x=0.05$ and 0.4 .

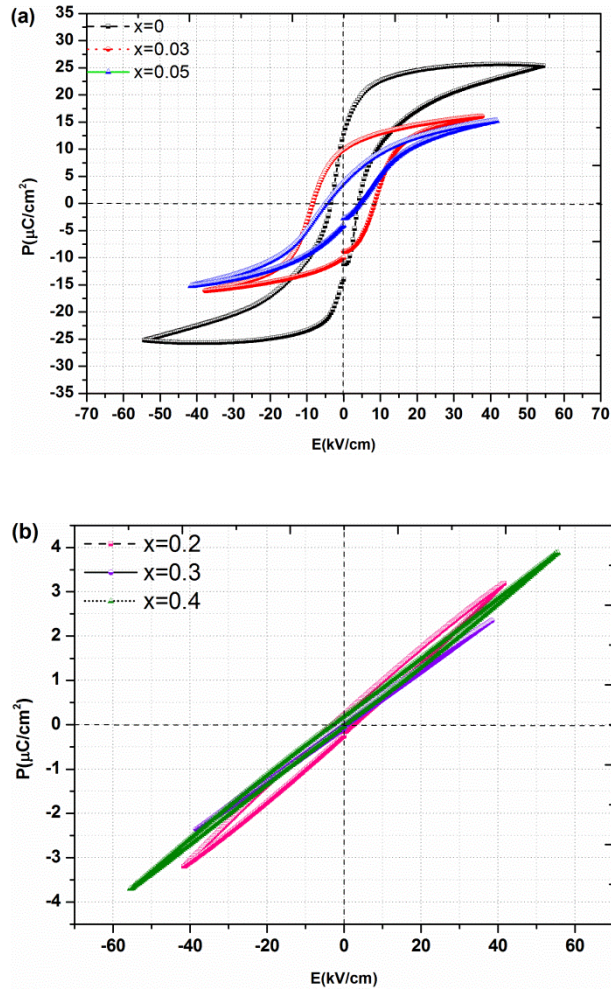


Figure 7. Polarisation-electric field, P-E, loops for (a) $x=0-0.05$ and (b) $x=0.2-0.4$.

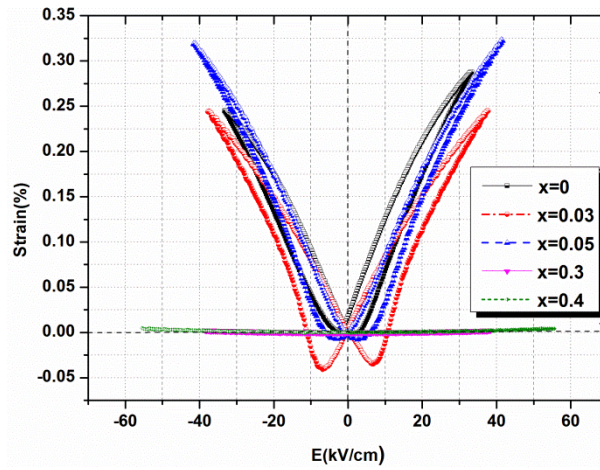


Figure 8. Electric field–strain behaviour for compositions $x=0, 0.03, 0.05, 0.2$ and 0.4 .